

Real-time monitoring of fat crystallization using pulsed acoustic spectroscopy and supervised machine learning

Original

Real-time monitoring of fat crystallization using pulsed acoustic spectroscopy and supervised machine learning / Metilli, L.; Morris, L.; Lazidis, A.; Marty-Terrade, S.; Holmes, M.; Povey, M.; Simone, E.. - In: JOURNAL OF FOOD ENGINEERING. - ISSN 0260-8774. - ELETTRONICO. - 335:(2022), p. 111192. [10.1016/j.jfoodeng.2022.111192]

Availability:

This version is available at: 11583/2969868 since: 2022-07-07T19:30:33Z

Publisher:

Elsevier Ltd

Published

DOI:10.1016/j.jfoodeng.2022.111192

Terms of use:

This article is made available under terms and conditions as specified in the corresponding bibliographic description in the repository

Publisher copyright

Elsevier postprint/Author's Accepted Manuscript

© 2022. This manuscript version is made available under the CC-BY-NC-ND 4.0 license
<http://creativecommons.org/licenses/by-nc-nd/4.0/>. The final authenticated version is available online at:
<http://dx.doi.org/10.1016/j.jfoodeng.2022.111192>

(Article begins on next page)

Real-time monitoring of fat crystallization using pulsed acoustic spectroscopy and supervised machine learning

*Lorenzo Metilli¹, Liam Morris¹, Aris Lazidis², Stephanie Marty-Terrade³, Melvin Holmes¹,
Megan Povey¹ and Elena Simone^{1,4}*

¹ School of Food Science and Nutrition, Food Colloids and Bioprocessing group, University of
Leeds, Woodhouse Lane, Leeds LS2 9JT, UK

² Nestlé Product Technology Centre Confectionery, Haxby Road, York YO31 8TA, UK

³ Nestlé Research, Vers-chez-les-Blanc, 1000 Lausanne 26, Switzerland

⁴ Department of Applied Science and Technology (DISAT), Politecnico di Torino, Torino (Italy)

KEYWORDS

Crystallization, Fats, Oils, Ultrasound, Machine Learning

ABSTRACT

Enhancing the control and yield of lipid crystallization is fundamental in several industrial areas, including pharmaceutical, cosmetic and food manufacturing. However, the multi-component nature of fats and oils poses a challenge in the understanding and control of the final product properties. While the crystallization of lipid has been extensively studied with offline techniques, online monitoring of the process would be highly advantageous, especially in large-scale sheared vessels. In this work, a novel method to calculate the solid fat content (SFC%) of crystallizing lipids under shear, based on an acoustic probe and supervised-machine learning, is presented. The temperature, composition and ultrasonic velocity of the samples, and the SFC(%) measured with nuclear magnetic resonance were used to develop a predictive model to calculate the SFC(%) during crystallization. Gaussian models showed the highest accuracy compared to linear and regression tree models (RMSE = 0.03 vs 0.7 and 0.25, respectively).

1. Introduction

The crystallization of lipids is a fundamental unit operation for several manufacturing industries, including pharmaceuticals (Jose & Netto, 2019), cosmetic (Duprat-De-Paule et al., 2018; Patel et al., 2021) and food (Rios et al., 2014). Recently, the use of crystalline fat to produce structured oils (oleogels) has gained significant attention from academia and industry alike, due to the potential to produce solid-like materials with low amounts of saturated fat and specific macroscopic properties (Patel & Dewettinck, 2016). Furthermore, oleogels may be used as precursors for the production of oil-continuous foams (Binks & Vishal, 2021) and emulsified oil foams (Brun et al., 2015; Goibier et al., 2019) that can find application as nutrients or drug delivery vehicles, or as structuring materials for food products. In all of the above examples, the properties of the fat crystals, such as crystal size, shape and polymorphism, significantly affect the stability and functionality (*e.g.*, drug delivery, oil binding capacity, air incorporation) of the final oleogel

40 material (Co & Marangoni, 2012; Heymans et al., 2017). The total amount of crystals, *i.e.* the solid
41 fat content (*SFC%*), is a general parameter strongly related to some macroscopic properties of fat-
42 based materials, such as the melting point, hardness and texture (Himawan et al., 2006). Hence,
43 monitoring *SFC%* during crystallization processes is important to determine when equilibrium
44 conditions are reached, and therefore maximize the yield of crystallization in industrial contexts.

45 The *SFC%* is routinely measured by means of nuclear magnetic resonance (NMR) (Cerdeira et al.,
46 2004), differential scanning calorimetry (DSC) (Foubert et al., 2008) or small-angle X-Ray
47 scattering (SAXS) (Ladd Parada et al., 2019). These techniques, however, are all off-line, requiring
48 the collection of a sample (not always a trivial operation, especially if the sample melting point is
49 close to ambient temperature) and some degree of sample preparation, which can significantly
50 affect the measurement. In the context of industrial large-scale crystallization, the issues related to
51 off-line analysis and sampling are tackled by applying process analytical technology (PAT) tools,
52 which enable real-time monitoring of the product properties, enhanced process understanding, and
53 the application of the so called “Quality by Design” (QbD) strategy (Rathore et al., 2010).
54 Common PAT tools used to monitor crystallization usually include *in situ* probes that exploit the
55 scattering or absorption of electromagnetic radiation (visible light, ultra-violet (UV) or infra-red)
56 by the sample to monitor phase transitions, polymorphic transformations or crystal morphology
57 (Hansen et al., 2017; Simone et al., 2015; Simone et al., 2019). In the case of industrial lipid
58 crystallization, online determination of the *SFC%* is highly sought, albeit presenting some
59 challenges. Fat crystals form a viscous three-dimensional network of aggregates with a fractal
60 pattern (Tang & Marangoni, 2008), whose quantification is non-trivial. Moreover, (partially)
61 crystalline fat is often opaque to electromagnetic radiation, limiting the analysis to the surface of
62 the sample. While oleogels (and hydrogels) are widely used in consumer products, at present there

are sparse examples of PAT tools applied to the manufacturing process of materials with similar properties (Bostijn et al., 2018; Pu et al., 2015).

The use of low-power ultrasound for studying the crystallization of lipids has been proposed as a non-invasive, non-destructive method since the 1980s (Hussin & Povey, 1984; McClements & Povey, 1988; McClements & Povey, 1987). Low-power ultrasound, *i.e.*, sound waves exceeding 20 kHz frequency, can penetrate opaque media, without causing physical and chemical changes in the sample. Moreover, it is relatively inexpensive compared to other spectroscopy techniques, and it is easily adaptable to different measuring configurations (Povey, 2017). The technique involves the propagation of a short (few microseconds) ultrasonic pulse from a transducer into the sample; this pulse is received by either another transducer on the other side of the measuring apparatus (pitch-and-catch mode) or it is reflected and received by the same emitting transducer (pulse-echo mode). The velocity of sound (c_{sample}) is then calculated from the travelled path length as a function of time and temperature. The acoustic attenuation (α), *i.e.*, the ratio of the amplitude of the sent and received pulse, may also be calculated. As both the velocity of sound and acoustic attenuation depend on the physicochemical properties of the sample, such as density and adiabatic compressibility, and the presence of heterogeneities, acoustic measurements can be used to monitor phase transitions such as crystallization and polymorphic transformations (Fairley & McClements, 1992; Klock et al., 2000; Miles et al., 1985). Several authors demonstrated the use of custom-made acoustic cells to study fat crystallization using acoustic signals, with particular emphasis on determining the *SFC*(%) (Birkhofer et al., 2008; Martini et al., 2005a, Martini et al., 2005b; Singh et al., 2002, Singh et al., 2004). Nevertheless, most of the previous works on fat crystallization were carried out in quiescent conditions, and/or with small sample volumes, thus

excluding the effect of shear and secondary nucleation on crystallization which are predominant on industrial scale (Agrawal & Paterson, 2015).

Despite its several advantages and ease of implementation, there are only sporadic examples in the literature on the use of acoustic probes as a PAT tool for studying lipid crystallization. The immersion probe described in Titiz-Sargut & Ulrich (2003), which featured two 2 MHz transducers in pitch-and-catch mode, was applied to the determination of the metastable zone width (MSZW) of coconut oil, and validated by optical back-reflectance measurements (ORM) (Chaleepa et al., 2010). The authors focused their study on the effect of different levels of shear, cooling rates and the presence of additives on the MSZW; however, no quantitative information on the *SFC%* of this lipid system was reported. Due to the complexity involved in the crystallization of lipids, such as the occurrence of melt-mediated polymorphic transformations, and the development of crystalline networks whose size range from nanometres to several hundreds of microns, the determination of the *SFC%* directly from acoustic parameters is non-trivial. Moreover, the large acoustic attenuation exhibited by crystalline fat results often in loss of the acoustic signal (Rigolle et al., 2018). One of the growing trends in the use of PAT tools is the implementation of machine learning (ML) algorithms to facilitate analysis of real-time data provided by sensors, and to enable prediction of material properties of interest based on training the algorithm with known outcomes (supervised machine learning) (Wasalathanthri et al., 2020). Examples of ML applications in the context of crystallization include the automatic detection of crystal aggregation from microscopic images (Ochsenbein et al., 2015), the real-time estimation of the crystal size distribution of 2D needle-shaped crystals from measurements of chord length and aspect ratio distributions (Szilágyi & Nagy, 2018) and the estimation of the 3D size distribution of plate-like particles using projections from multiple cameras (Jaeggi et al., 2021).

The approach can be extended to the actual control of crystallization processing, for example through the use of convolutional neural network (CNN) feedback control to dissolve undesired precipitated impurities during the crystallization of active pharmaceutical ingredients (APIs) (Salami et al., 2021). Recently, ML has been applied to ultrasonic reflectance measurements to monitor the mixing process in a large-scale vessel (Bowler et al., 2020; Bowler & Watson, 2021).

In this work, a novel technique for estimating the *SFC%*, based on a custom-built acoustic probe (Morris et al., 2021) and supervised machine learning is presented. This immersion acoustic probe was used as a PAT sensor to monitor the crystallization of a cocoa butter/sunflower oil oleogel system, in a 1L scale vessel and under shear. Stirring was maintained constant throughout the whole temperature profile. Cocoa butter and sunflower oil are both ingredients widely used in food, cosmetic and pharmaceutical applications (Metilli et al., 2021). The ultrasonic data was validated with light turbidimetry, and the *SFC%* of the crystallized oleogel was measured with offline pulsed NMR (*p*NMR) at equilibrium conditions and specific temperatures. Finally, supervised machine learning was applied to develop a predictive model based on the acoustic parameters and the results of *p*NMR, enabling the calculation of *SFC%* based on the velocity of sound, sample composition and temperature.

2. Materials and Methods

2.1 Cocoa butter–based oleogels

Refined, bleached and deodorized cocoa butter (CB) and high-oleic sunflower oil (HOSO) were kindly provided by Nestlé PTC Confectionery (York, UK) and used without any further purification. CB was melted at 65 °C for one hour, and then mixed with HOSO at 9%, 11%, 13% and 15% concentration by weight. HOSO contains usually the following fatty acids (by weight):

86% oleic acid, 5% stearic acid, 3% linoleic acid, 3% palmitic acid, 1.5% behenic acid, and 0.7% arachidic acid. CB normally contains by a weight about 26% palmitic acid, 36% stearic acid, 34% oleic acid, 2.7% linoleic, and 0.9% arachidic acid.

2.2 Fat crystallization rig

The CB-HOSO mixture (900 g) was transferred to a jacketed crystallization vessel (capacity *ca.* 1 L, diameter 15 cm) (Radley, UK) connected to a Huber Ministat 230 thermostat (Huber, Germany), filled with silicone oil as a heating/cooling medium. The sample was stirred continuously at 200 rpm with a DLH overhead stirrer (VELP Scientifica, Italy), equipped with an anchor-shaped mixer (8 cm diameter). A Pt-100 temperature probe (Omega Engineering, UK), placed in the vessel, was used to monitor the sample temperature during the experiment. The crystallization process was followed using a Control 4000 turbidity meter (Optek, Germany) fitted with an ASD12-N absorption probe, which measured light transmittance and absorbance. Finally, the velocity of sound and the acoustic attenuation of the crystallizing mixture were measured using a custom acoustic probe, recently described in literature (Morris et al., 2021), with some design modifications. Briefly, the probe comprised a 2.25 MHz broadband transducer coupled with a Rexolite buffer rod (Sonatest model RDT5025, Sonatest, UK), and a stainless-steel acoustic reflector plate. This probe was manufactured in an ‘L’ shape configuration. The probe was connected to a UT320 pulser/receiver (UTEX scientific instruments inc., Canada) and a HDO3034 digital oscilloscope (Teledyne LeCroy, USA). A schematic of the equipment is shown in Figure 1.

The thermal profile of the experiment was set to the following: Equilibration of the fat blend mixture at 45 °C for 10 minutes, cooling to 0 °C at a nominal rate of –0.5 °C/min and holding at

0°C for 3 hours. The sample was then heated back to 45 °C at 1 °C/min. The process temperature and the acoustic waveforms were collected using an in-house script developed with MATLAB2021a (MathWorks, USA). Measurements were collected every 10 seconds. Each experiment was repeated three times.

2.3 Determination of the acoustic parameters

2.3.1 Velocity of Sound

Figure contains a diagram describing the design of the acoustic probe, and an example of waveform acquired from the oscilloscope with MATLAB.

The ultrasonic pulse generated from the transducer travels through the buffer rod, and it is partially reflected at the buffer rod/sample interface, due to the acoustic impedance mismatch (*i.e.*, the difference in the product of density and velocity of sound of the two materials). The pulse is then received back by the transducer after a time Δt_1 , shown in Figure as the blue trace. Part of the initial pulse, however, is transmitted through the sample, and it is reflected by the stainless-steel reflector to the transducer after a time Δt_2 (Figure , red trace). In order to calculate the velocity of sound in the sample, the time of flight in the sample is required. To calculate it, the initial value of Δt_1 and Δt_2 were first determined with MATLAB from the original waveform, using the leading-edge method (*i.e.*, detecting the arrival time of the pulse envelope when it crosses a set voltage threshold). Afterwards, the shifts of the pulses' position ($\Delta\Delta t_1$ and $\Delta\Delta t_2$) during the experiment were calculated with the cross-correlation function (*xcorr*) implemented in MATLAB. This function provides an estimate of the correlation between each analysed waveform and a reference waveform, returning the intensity of the correlation value as a function of time units. The position of the maximum peak of this calculated vector corresponds to the time delay between two pulses. This method proved to be more robust in the analysis of the set of waveforms compared to applying

the leading-edge technique on all collected waveforms. This is because the pulse envelop was subject to distortion due to frequency dependent signal attenuation through the experiment. The variation in the sample time of flight ($\Delta\Delta t_3$) was then calculated with Equation 1:

$$\Delta\Delta t_3 = \Delta\Delta t_2 - \Delta\Delta t_1 \quad (\text{Eq. 1})$$

In order to obtain an accurate value of the velocity of sound, however, it was necessary to determine the path length dependence on the temperature with a calibration experiment. The velocity of sound in distilled water (c_{water}) with respect to temperature (T) may be calculated using a fifth-order polynomial, as first described by Chávez et al. (1985) (Equation 2):

$$c_{\text{water}} = 3.16 \cdot 10^{-9}T^5 - 1.48 \cdot 10^{-6}T^4 + 3.35 \cdot 10^{-4}T^3 - 5.81 \cdot 10^{-2}T^2 + 5.04 \cdot T + 1.40 \cdot 10^3 \quad (\text{Eq. 2})$$

The shift in the time of flight in distilled water ($\Delta\Delta t_{3,\text{water}}$) was then measured between 50 °C and 5°C, using a -0.01 °C/min cooling rate to allow the probe to reach thermal equilibrium with the surrounding medium. The corresponding experimental path length ($L_{\text{calibrated}}$) was calculated with Equation 3

$$L_{\text{calibrated}} = \Delta\Delta t_{3,\text{water}} \times c_{\text{water}} \quad (\text{Eq. 3})$$

The dependence of the path length on the temperature was then obtained by fitting a fifth-order polynomial to $L_{\text{calibrated}}$ against the temperature (Figure).

The coefficients estimated for the path length calculation were then used to accurately calculate the velocity of sound during the crystallization experiments with Equation 4

$$c_{\text{sample}} = \frac{L_{\text{calibrated}}}{\Delta\Delta t_3} \quad (\text{Eq. 4})$$

2.3.2 Acoustic Attenuation

The acoustic attenuation quantifies the acoustic power absorbed and scattered by the sample, and is affected by several factors, including the onset of phase transitions and scattering phenomena

generated by the presence of dispersed objects in the sample (McClements & Povey, 1992). In this work, the acoustic attenuation was used to detect the onset of crystal growth and dissolution during the crystallization experiments. The acoustic attenuation was calculated according to Equation 5

$$\alpha = -20 \log \frac{A}{A_0} \quad (\text{Eq. 5})$$

where A and A_0 are the peak-to-peak amplitudes of the sample signal during the experiment, and at the start of the experiment, respectively.

2.3.3 Solid Fat Content

The solid fat content ($SFC\%$), defined as the mass fraction of solid to liquid material in a fat blend, was calculated by applying a prediction model, developed with the Regression Learner App in MATLAB2021a, (MathWorks, USA). Regression Learner is a supervised machine-learning utility, where a regression algorithm is applied to an observation matrix and compared with a response matrix. The observation matrix comprised the temperature (T), velocity of sound in the sample (c_{sample}) and the amount of added cocoa butter ($CB\%$) for each crystallization experiment; the response matrix contained the $SFC\%$ values, measured with pNMR, between 5 and 45 °C for the respective samples. The velocity of sound and temperature of pure sunflower oil were also added to the observation matrix, with a corresponding solid fat content of 0%. The sunflower oil data was included in the model to provide information on the behaviour of a sample without any crystallizing material in the explored experimental conditions. Three models available in the Regression Learner App were tested for training of the dataset, and their predictive ability were compared: “Linear”, “Fine Tree” and “Gaussian Process Regression–Rational Quadratic”. The Linear model uses a linear regression to fit the data from the observation matrix. The “Fine Tree” model, instead, is a type of nonlinear model based on regression trees, which applies a recursive

partition of the observation matrix to improve the prediction of the response value. Lastly, the Gaussian Process Regression model, which is also nonlinear, works by predicting the probability distribution of responses for each parameter in the observation matrix. Model cross-validation was performed using the in-built function in the Regression Learner App (5-fold validation setting). Briefly, the software divides the dataset into a number of sub-sets of the same size, trains the predictive model on all sub-sets except one, which is used as test data. This process is repeated until all sub-sets have been used as test data once (Bosnić & Kononenko, 2009). The accuracy of all iterations is calculated as R^2 , RMSE and other statistical parameters. In the discussion, the Root Mean Square Error values (RMSE) were compared to select the most accurate predictive model. In addition to the predictive model, an equation that estimates the equilibrium *SFC%* as function of the temperature and the concentration of CB in sunflower oil was determined using the *Curve Fitting Tool* in MATLAB2021a. A custom equation based on literature was used to fit the experimental data using the *NonlinearLeastSquares* method; R^2 , RMSE and 95% confidence intervals for each estimated parameters were also calculated.

2.4 Pulsed Nuclear Magnetic Resonance (pNMR)

The solid fat content (*SFC%*) of the CB-HOSO mixtures was determined with *pNMR* using a Bruker Minispec NMR (Bruker, Switzerland). The samples were collected at the end of the crystallization experiment, transferred to a 10 mm inner diameter NMR tube and stored in a fridge at 4 °C. The *SFC%* was measured between 5 and 45 °C, in steps of 5 °C. During the experiment, the NMR tube was left to equilibrate for 90 minutes for each temperature step. The measurements were carried out in triplicates. The resulting *SFC(%)* vs. temperature data was fitted using a Gompertz-type model (Farmani, 2015) to obtain the *SFC(%)* as a function of the temperature and CB%.

3. Results and Discussion

3.1 Fat crystallization monitored by PAT tools

The crystallization of one 9% CB w/w in HOSO sample, monitored with turbidity and the acoustic probe, is shown in Figure 4.

While some variability among the three experiments conducted for each CB concentration was observed, (particularly in the crystallization temperature and the absolute values of acoustic attenuation) the trends observed for all CB/HOSO samples were similar. In particular, for the experiment shown in Figure 4a, four regions could be identified. Between 0 and 115 minutes (region I of Figure 4a) the temperature of the sample followed the cooling profile, from 45 °C to 5°C, accompanied by an increase in the velocity of sound, from 1390 to 1510 m/s, due to the negative velocity coefficient with respect to temperature (McClements & Povey, 1992). After 115 minutes, when the sample temperature reached 5 °C, the onset of nucleation was detected by a sharp decrease in the light transmittance, due to the sample becoming turbid (region II). Simultaneously, the light absorbance increased, exhibiting two distinct steps: a first, modest increase occurring between 115 and 129 minutes, and a larger increase after 129 minutes. Interestingly, the acoustic attenuation and the velocity of sound were responsive to the second step only, with a delay in detecting the onset of crystallization of *ca.* 14 minutes. This behaviour was consistently observed across all CB % w/w concentrations (Figure S1 of Supporting Information), and reported also in previous works (Martini et al., 2005b; Singh et al., 2002). The sheared crystallization of CB/HOSO mixtures was thoroughly investigated in a recent publication, reporting that cocoa butter crystallized as spherical aggregates of crystalline nanoplatelet (CNPs) in the $\beta(V)$ form (Metilli et al., 2021) (Figure 5). Additional characterization is provided in the Supporting Information (Figure S2).

It is hypothesized, however, that CB first nucleated as a metastable polymorph (α or β') and then transformed into the $\beta(V)$ structure during the experiments. It might be that the change in compressibility and/or density associated to the formation of a liquid crystal structure – most likely the α polymorph – were too small to be detected by the acoustic probe used in this work (Ladd Parada et al., 2019). On the other hand, the nucleation and the growth of the $\beta(V)$ crystals and the consequent development of the fat crystal network were clearly detected in both the velocity of sound and acoustic attenuation (at 129 minutes). As the velocity of sound depends strongly on the temperature, the first derivative with respect to temperature was calculated to better discriminate the effect of crystal nucleation on this acoustic parameter (Figure 4b). Before the appearance of fat crystals, when the change in the velocity of sound was only dependent on the temperature, the calculated first derivative was zero; whereas, upon growth of the CB crystal network, the value of this parameter changed significantly. Variations in the first derivative occurred at the same time with the increase of the acoustic attenuation, which was caused by (a) scattering by fat crystals and (b) additional attenuation mechanisms associated with the space filling interconnected fat crystals, which also affected the overall compressibility of the system through the appearance of an additional ‘frame modulus’ (Povey, 2017). Finally, fat crystal nucleation might release a high amount of latent heat of solidification. In the case of the experiment of Figure 4a, such exothermic process increased the process temperature from 3.2 °C to 5.65 °C (130-137 minutes). While this temperature perturbation did not affect the signal from the turbidity probe or the acoustic attenuation, it did affect the velocity of sound, which is strongly dependent on the sample temperature.

After nucleation of the $\beta(V)$ polymorph, the crystallization process of Figure 4a proceeded until 275 minutes (region III), when the sample temperature reached *ca.* 1.5 °C, which corresponded to

the thermal equilibrium of the whole setup. In this time the acoustic attenuation kept increasing, following a similar trend to the light absorbance. The velocity of sound also increased, but mostly due to the change in temperature. Nevertheless, it is worth noticing in Figure 4b that the appearance of fat crystals determined an increase in the noise of the first derivative of the velocity of sound, albeit its mean value was still around zero.

After reaching equilibrium at around 275 minutes, the sample was heated back to 45 °C (region IV). A focus on this region of the experiment is displayed in Figure 4c. In the heating step between 1.5 °C to 15 °C (from 280 minutes to 315 minutes), a decrease in the velocity of sound linearly proportional to the decrease in temperature was observed. At the same time, a moderate decrease in the acoustic attenuation happened, potentially linked to a decrease in the *SFC*% of the crystallized sample.

Further increase in the sample temperature (from 315 to 330 minutes, 15 °C to 25 °C) resulted in the complete melting of the fat crystalline network, which was evident in the sharp increase in light transmittance and in the decrease in light absorbance, as well as acoustic attenuation. It is worth noticing that both techniques detected full dissolution at the same time, around 327 minutes. The velocity of sound presented a steeper decline in correspondence to the full melting; this was clearly observable in the calculated first derivative.

Upon complete remelting of the sample (330 minutes – 350 minutes) all parameters returned to their values prior to crystallization.

This set of experiments showed that the tested acoustic probe could be used to monitor crystallization processes, although it seemed less sensitive than light turbidimetry to the detection of early nucleated crystals, perhaps due to their liquid crystalline nature.

Experiments carried out with a higher weight % of CB showed similar trends for the acoustic and light signals. The velocity of sound of the crystallized oleogels at different % w/w of added CB, between 5 and 35°C, is shown in Figure 6.

In agreement with previous literature (McClements & Povey, 1992), the velocity of sound of the crystallized oleogels increased, for the same range of temperatures, with increasing CB % w/w (approximately by 10 m/s every 2 % of CB). From Figure 6 it can be noted that, between 20 and 25°C, the velocity of sound of all samples decreased steeply, due to the oleogels melting. It can be appreciated that such decrease occurred at lower temperatures for lower CB concentrations, in accordance with the lower melting point of the oleogels. Once liquid, the oleogels then displayed the same velocity of sound of the sunflower oil.

The acoustic attenuation measured at equilibrium also increased with the amount of CB contained in the oleogel, as shown in **Table 1**. In fact, higher concentrations of crystalline solids scattered more sound and attenuated it. The relatively large standard deviation of the acoustic attenuation for the 9% CB w/w sample, and its non-linear increase with higher concentrations of CB w/w, however, prompts further work to establish a more robust relationship with the amount of solid fat in the sample. In fact, the relationship between acoustic attenuation, *SFC*(%) and the crystal size and shape is challenging to elucidate (Martini et al., 2005a).

The solid fat content (*SFC*%) of the CB/HOSO samples as a function of temperature was measured with *p*NMR at the end of the crystallization step (Figure 7). Samples were collected directly from the vessel to ensure direct comparison with the performed experiments.

By inspecting the *SFC*% values at 5 °C, it can be noted that all samples displayed a lower *SFC*% compared to the total amount of added cocoa butter. This is because the main triacylglycerides species that are solid at ambient temperature, 1,3-dipalmitoyl-2-oleoyl-glycerol (POP), 1,3-

distearoyl-2-oleoyl-glycerol (SOS) and 1-palmitoyl-2-oleoyl-3-stearoyl-glycerol (POS), constitute about 80% w/w of cocoa butter, while the remaining 20% comprises mono- and diglycerides, phospholipids, sterols and free fatty acids that are liquid at ambient conditions (Dimick, 1991). It is worth noticing that the *p*NMR measurements present an average standard deviation of 0.101%, which is a more than acceptable value for industrial applications (particularly the confectionary sector).

The *SFC*(%) values at equilibrium were fitted using a Gompertz-type model, similar to the one described in Farmani (2015) (Equation 6):

$$SFC(\%)(T, CB) = (b_0 + b_1 CB) e^{-e^{\frac{-(T - (b_{01} + (b_{11} CB)))}{c}}} \quad (\text{Eq. 6})$$

where *T* is the sample temperature in °C, *CB* is the concentration (w/w) of added cocoa butter, and $b_0 = 1.24$, $b_1 = 73$, $b_{01} = 13.48$, $b_{11} = 38.5$ and $c = -4.66$ are the coefficient determined via interpolation in MATLAB. The R^2 of the fitting was equal to 0.9965 with a *RMSE* of 0.2324% (95% confidence intervals for each parameter are shown in supporting information Table S1), which is still acceptable for industrial purposes.

This fit enabled calculation of the equilibrium *SFC*(%) as a function of temperature and *CB* concentration, which can be used in combination with the predictive models determined in the next section for oleogels with composition ranging from 9 to 15% of *CB*.

3.2 Solid fat content predicted by Regression Learner model

The measured *SFC*(%) with *p*NMR, and the predicted *SFC*(%) obtained with the Regression Learner models is displayed in Figure 8.

It can be noticed how the Linear model showed inaccuracies both when the sample was in the melted state (high temperatures), as well as in its crystallized phase, at all concentrations. This

could be ascribed to the non-linear dependence of the $SFC(\%)$ with respect to temperature, as already highlighted in Figure 7. When considering the Fine Tree model, the accuracy generally improved, however still displaying some errors in predicting the $SFC(\%)$ of the oleogels, in particular between 15 and 25 °C. Finally, the GPR model showed the best predictive accuracy, for all samples and temperatures, with an RMSE value almost one order of magnitude lower compared to the other two models. Such improvement could stem from the similarity between the Gompertz-type $SFC(\%)$ dependence with temperature (Equation 6) and the gaussian-type distribution function (also exponential). Therefore, the GPR model was selected to predict the SFC% evolution during fat crystallization, as shown in Figure .

The increase in the predicted value of the $SFC\%$ in the oleogel matched the increase in the acoustic attenuation at 130 minutes, reaching 5% over few minutes and then levelling to a value of about 7.6%, very close to the equilibrium $SFC\%$ at such temperature (as shown in Figure 7). During the heating phase, the $SFC\%$ started decreasing, falling sharply to 0% when the temperature was raised above 20 °C and remaining constant thereafter, until the end of the experiment. Therefore, in contrast with previous research, the approach presented in this work only requires measuring velocity of sound, the temperature, and the $SFC(\%)$ measured with $pNMR$ on samples on the concentration of interest. The $SFC(\%)$ is then rapidly and accurately predicted from the ultrasonic probe data under realistic operating conditions (*i.e.*, under shear and with large sample volumes). The predicted $SFC\%$ for the samples at different CB % was plotted as a function of temperature in Figure .

By inspecting the cooling profile, it can be noted that crystal growth, signalled by the increase in $SFC\%$, occurred at higher crystallization temperatures for oleogels containing higher % of CB, as also reported previously in Metilli et al. (2021) for this type of system. Whereas, by inspecting the

heating profile, the *SFC*% decreased with the temperature with the same trend observed with *p*NMR. The estimated values of *SFC*% at 5 °C during heating were 7.3, 8.7, 10.2 and 11.7% for the 9, 11, 13 and 15% CB samples, respectively. These values are very close to the equilibrium *SFC*% measured with *p*NMR at the same temperature (7.6, 8.5, 10.3 and 11.7%) indicating the reliability of the predictive model built. Furthermore, both *p*NMR and acoustic spectroscopy showed agreement that at 25 °C all samples returned to the full liquid state.

This work presents a prototype of an acoustic in situ probe, coupled with a reliable machine learning-based predictive model, for online monitoring of oleogels crystallization. The probe could provide useful quantitative information on the evolution of crystallization processes in an industrial setting with minimal investment cost and calibration experiments. Furthermore, due to the versatility of acoustic probes, the design of the hardware could be optimized in order to allow effective measurements even in different fluid-dynamic environment (e.g., different crystallizers designs, commercial tempering equipment).

4. Conclusions

In this work, the crystallization of cocoa butter-based oleogels was characterized qualitatively and quantitatively using a custom-built immersion probe based on pulsed acoustic spectroscopy. The *SFC*% of the oleogel during crystallization was estimated through a predictive model developed with supervised machine learning. Such method uses the acoustic parameters (*i.e.*, velocity of sound) collected from the immersion probe, the sample temperature and composition, and the *SFC*% measured with *p*NMR. The predicted *SFC*% and its evolution during the shear crystallization of the CB/HOSO mixtures was in agreement with the nucleation and development of crystalline fat, as corroborated by light turbidimetry and acoustic attenuation. A comparison

between several predictive models showed that Gaussian Process Regression model was the most accurate in describing the *SFC%* both prior and during crystallization. The *SFC%* value increased steeply during crystal growth, with a final value close to 80% by weight of the added cocoa butter in the mixture, with a similar trend to the acoustic attenuation. The *SFC%* then returned to 0% close to the melting point of the oleogel, in agreement with the melting profile measured with *p*NMR. Moreover, this work highlighted that turbidimetry was more sensitive in detecting the nucleation of lipid crystals, whereas the acoustic probe was more responsive to the crystal growth process. This difference could be ascribed to the liquid-crystalline nature of the metastable lipid polymorph that developed during nucleation, for which the change in density and compressibility may be too small to be measured by the current acoustic probe. Using a different frequency transducer might increase the sensitivity of the ultrasonic probe to crystal nucleation; however, this might result in excessive signal attenuation at equilibrium conditions, at which the *SFC%* needs to be calculated. In summary, the results presented in this work demonstrate the feasibility of implementing acoustic probes as PAT tools, in combination with supervised machine learning, to improve the oleogel crystallization yield through the timely and accurate monitoring of the *SFC%*.

ASSOCIATED CONTENT

Supporting Information.

PAT tools plot of 9, 11, 13 and 15% w/w CB in HOSO samples focused on nucleation of CB crystals (Figure S1). SAXS and WAXS patterns, DSC and CryoSEM images of a 15% w/w CB in HOSO oleogel sample (Figure S2).

420 AUTHOR INFORMATION

421

422 **Corresponding Author**

423 Prof. Elena Simone

424 Elena.simone@polito.it

425

426 **Author Contributions**

427 The manuscript was written through contributions of all authors. All authors have given approval
428 to the final version of the manuscript.

429

430 **Funding Sources**

431 Centre for Doctoral Training in Soft Matter and Functional Interfaces (Grant ref. no.
432 EP/L015536/1).

433 Royal Society (Grant ref. no. INF\R2\192018).

434 Royal Academy of Engineering (Grant ref. no. IF/192031).

435 **ACKNOWLEDGMENTS**

436 The authors would like to acknowledge the Engineering and Physical Sciences Research Council
437 funded Centre for Doctoral Training in Soft Matter and Functional Interfaces, grant ref. no.
438 EP/L015536/1 as well as Nestlé PTC Confectionery (York, UK) for the pulsed NMR analysis, and
439 the financial and writing support. E.S. also acknowledges Royal Society (Grant ref. no.

440 INF\R2\192018) and Royal Academy of Engineering (Grant ref. no. IF/192031) for additional
441 funding.

442 ABBREVIATIONS

443 CB cocoa butter, GPR gaussian process regression, HOSO high oleic sunflower oil, ML machine
444 learning, SFC solid fat content, PAT process analytical technologies, *p*NMR pulsed nuclear
445 magnetic resonance.

446 REFERENCES

447 Agrawal, S. G., & Paterson, A. H. J. (2015). Secondary Nucleation: Mechanisms and Models.
448 *Chemical Engineering Communications*, 202(5), 698–706.
449 <https://doi.org/10.1080/00986445.2014.969369>

450 Rigolle, A., Van Den Abeele, K. and Foubert, I. (2018). Conventional and New Techniques to
451 Monitor Lipid Crystallization. In Crystallization of Lipids, K. Sato
452 (Ed.). <https://doi.org/10.1002/9781118593882.ch17>

453 Binks, B. P., & Vishal, B. (2021). Particle-stabilized oil foams. *Advances in Colloid and Interface*
454 *Science*, 291, 102404. <https://doi.org/10.1016/j.cis.2021.102404>

455 Birkhofer, B. H., Jeelani, S. A. K., Windhab, E. J., Ouriev, B., Lisner, K.-J., Braun, P., & Zeng,
456 Y. (2008). Monitoring of fat crystallization process using UVP–PD technique. *Flow*
457 *Measurement and Instrumentation*, 19(3–4), 163–169.
458 <https://doi.org/10.1016/j.flowmeasinst.2007.08.008>

459 Bosnić, Z., & Kononenko, I. (2009). An overview of advances in reliability estimation of
460 individual predictions in machine learning. *Intelligent Data Analysis*, 13(2), 385–401.

461 <https://doi.org/10.3233/IDA-2009-0371>

462 Bostijn, N., Hellings, M., Van Der Veen, M., Vervaet, C., & De Beer, T. (2018). In-line UV
463 spectroscopy for the quantification of low-dose active ingredients during the manufacturing
464 of pharmaceutical semi-solid and liquid formulations. *Analytica Chimica Acta*, 1013, 54–62.
465 <https://doi.org/10.1016/j.aca.2018.02.007>

466 Bowler, A. L., Bakalis, S., & Watson, N. J. (2020). Monitoring Mixing Processes Using Ultrasonic
467 Sensors and Machine Learning. *Sensors*, 20(7), 1813. <https://doi.org/10.3390/s20071813>

468 Bowler, A. L., & Watson, N. J. (2021). Transfer learning for process monitoring using reflection-
469 mode ultrasonic sensing. *Ultrasonics*, 115(May), 106468.
470 <https://doi.org/10.1016/j.ultras.2021.106468>

471 Brun, M., Delamplé, M., Harte, E., Lecomte, S., & Leal-Calderon, F. (2015). Stabilization of air
472 bubbles in oil by surfactant crystals: A route to produce air-in-oil foams and air-in-oil-in-
473 water emulsions. *Food Research International*, 67, 366–375.
474 <https://doi.org/10.1016/j.foodres.2014.11.044>

475 Cerdeira, M., Candal, R.J., Herrera, M. L. (2004). Analytical Techniques for Nucleation Studies
476 in Lipids : Advantages and Disadvantages. *Journal of Food Science*, 69(9), R185–R191.

477 Chaleepa, K., Szepes, A., & Ulrich, J. (2010). Metastable zone determination of lipid systems:
478 Ultrasound velocity versus optical back-reflectance measurements. *European Journal of*
479 *Lipid Science and Technology*, 112(5), 565–573. <https://doi.org/10.1002/ejlt.200900225>

480 Chávez, M., Sosa, V., & Tsumura, R. (1985). Speed of sound in saturated pure water. *Journal of*
481 *the Acoustical Society of America*, 77(2), 420–423. <https://doi.org/10.1121/1.391861>

482 Co, E. D., & Marangoni, A. G. (2012). Organogels: An alternative edible oil-structuring method.
 483 *JAACS, Journal of the American Oil Chemists' Society*, 89(5), 749–780.
 484 <https://doi.org/10.1007/s11746-012-2049-3>

485 Dimick, P. S. (1991). Principles of cocoa butter crystallization. *Manufacturing Confectioner*,
 486 71(5), 115–125.

487 Duprat-De-Paule, S., Guilbot, J., Roso, A., Cambos, S., & Pierre, A. (2018). Augmented bio-based
 488 lipids for cosmetics. *OCL - Oilseeds and Fats, Crops and Lipids*, 25(5).
 489 <https://doi.org/10.1051/ocl/2018036>

490 Fairley, P., & McClements, D. J. (1992). Frequency scanning ultrasonic pulse echo reflectometer.
 491 *Ultrasonics*, 30(6), 403–405.

492 Farmani, J. (2015). Modeling of solid fat content of chemically interesterified fully hydrogenated
 493 soybean oil and canola oil blends as a function of temperature and saturated fatty acids.
 494 *Journal of Food Measurement and Characterization*, 9(3), 281–289.
 495 <https://doi.org/10.1007/s11694-015-9233-8>

496 Fernández-Moya, V., Martínez-Force, E., & Garcés, R. (2000). Identification of triacylglycerol
 497 species from high-saturated sunflower (*Helianthus annuus*) mutants. *Journal of Agricultural*
 498 *and Food Chemistry*, 48(3), 764–769. <https://doi.org/10.1021/jf9903861>

499 Foubert, I., Fredrick, E., Vereecken, J., Sichien, M., & Dewettinck, K. (2008). Stop-and-return
 500 DSC method to study fat crystallization. *Thermochimica Acta*, 471(1–2), 7–13.
 501 <https://doi.org/10.1016/j.tca.2008.02.005>

502 Goibier, L., Pillement, C., Monteil, J., Faure, C., & Leal-Calderon, F. (2019). Emulsification of

503 non-aqueous foams stabilized by fat crystals: Towards novel air-in-oil-in-water food colloids.
504 *Food Chemistry*, 293, 49–56. <https://doi.org/10.1016/j.foodchem.2019.04.080>

505 Hansen, T. B., Simone, E., Nagy, Z., & Qu, H. (2017). Process Analytical Tools to Control
506 Polymorphism and Particle Size in Batch Crystallization Processes. *Organic Process*
507 *Research and Development*, 21(6), 855–865. <https://doi.org/10.1021/acs.oprd.7b00087>

508 Heymans, R., Tavernier, I., Dewettinck, K., & Van der Meeren, P. (2017). Crystal stabilization of
509 edible oil foams. *Trends in Food Science and Technology*, 69, 13–24.
510 <https://doi.org/10.1016/j.tifs.2017.08.015>

511 Himawan, C., Starov, V. M., & Stapley, A. G. F. (2006). Thermodynamic and kinetic aspects of
512 fat crystallization. *Advances in Colloid and Interface Science*, 122, 3–33.
513 <https://doi.org/10.1016/j.cis.2006.06.016>

514 Hussin, A. B. B. H., & Povey, M. J. W. (1984). A study of dilatation and acoustic propagation in
515 solidifying fats and oils: II. Experimental. *Journal of the American Oil Chemists' Society*,
516 61(3), 560–564. <https://doi.org/10.1007/BF02677032>

517 Jaeggi, A., Rajagopalan, A. K., Morari, M., & Mazzotti, M. (2021). Characterizing Ensembles of
518 Platelike Particles via Machine Learning. *Industrial & Engineering Chemistry Research*,
519 60(1), 473–483. <https://doi.org/10.1021/acs.iecr.0c04662>

520 Jose, J., & Netto, G. (2019). Role of solid lipid nanoparticles as photoprotective agents in
521 cosmetics. *Journal of Cosmetic Dermatology*, 18(1), 315–321.
522 <https://doi.org/10.1111/jocd.12504>

523 Kloek, W., Walstra, P., & Van Vliet, T. (2000). Nucleation kinetics of emulsified triglyceride

524 mixtures. *JAOCS, Journal of the American Oil Chemists' Society*, 77(6), 643–652.
 525 <https://doi.org/10.1007/s11746-000-0104-7>

526 Ladd Parada, M., Povey, M. J., Vieira, J., Rappolt, M., & Ries, M. E. (2019). Early stages of fat
 527 crystallisation evaluated by low-field NMR and small-angle X-ray scattering. *Magnetic*
 528 *Resonance in Chemistry*, 57(9), 686–694. <https://doi.org/10.1002/mrc.4860>

529 Lipp, M., Simoneau, C., Ulberth, F., Anklam, E., Crews, C., Brereton, P., ... Wiedmaier, C.
 530 (2001). Composition of genuine cocoa butter and cocoa butter equivalents. *Journal of Food*
 531 *Composition and Analysis*, 14(4), 399–408. <https://doi.org/10.1006/jfca.2000.0984>

532 Martini, S., Bertoli, C., Herrera, M. L., Neeson, I., & Marangoni, A. (2005a). Attenuation of
 533 ultrasonic waves: Influence of microstructure and solid fat content. *JAOCS, Journal of the*
 534 *American Oil Chemists' Society*, 82(5), 319–328. [https://doi.org/10.1007/s11746-005-1073-](https://doi.org/10.1007/s11746-005-1073-6)
 535 6

536 Martini, S., Bertoli, C., Herrera, M. L., Neeson, I., & Marangoni, A. (2005b). In situ monitoring
 537 of solid fat content by means of pulsed nuclear magnetic resonance spectrometry and
 538 ultrasonics. *JAOCS, Journal of the American Oil Chemists' Society*, 82(5), 305–312.
 539 <https://doi.org/10.1007/s11746-005-1071-8>

540 McClements, D. J. J., & Povey, M. J. W. (1988). Ultrasonic velocity measurements in some liquid
 541 triglycerides and vegetable oils. *Journal of the American Oil Chemists' Society*, 65(11),
 542 1787–1790. <https://doi.org/10.1007/BF02542383>

543 McClements, D. J., & Povey, M. J. W. (1992). Ultrasonic analysis of edible fats and oils.
 544 *Ultrasonics*, 30(6), 383–388. [https://doi.org/10.1016/0041-624X\(92\)90094-3](https://doi.org/10.1016/0041-624X(92)90094-3)

545 McCLEMENTS, D. J., & POVEY, M. J. W. (1987). Solid fat content determination using
 546 ultrasonic velocity measurements. *International Journal of Food Science & Technology*,
 547 22(5), 491–499. <https://doi.org/10.1111/j.1365-2621.1987.tb00514.x>

548 Metilli, L., Lazidis, A., Francis, M., Marty-Terrade, S., Ray, J., & Simone, E. (2021). The Effect
 549 of Crystallization Conditions on the Structural Properties of Oleofoams Made of Cocoa Butter
 550 Crystals and High Oleic Sunflower Oil. *Crystal Growth & Design*, 21(3), 1562–1575.
 551 <https://doi.org/10.1021/acs.cgd.0c01361>

552 Miles, C. A., Fursey, G. A. J., & Jones, R. C. D. (1985). Ultrasonic estimation of solid/liquid ratios
 553 in fats, oils and adipose tissue. *Journal of the Science of Food and Agriculture*, 36(3), 215–
 554 228. <https://doi.org/10.1002/jsfa.2740360312>

555 Morris, L., Simone, E., Glover, Z. J., Powell, H., Marty-Terrade, S., Francis, M., & Povey, M. J.
 556 (2021). Dynamic monitoring of glycine crystallisation with low power ultrasound reflection
 557 spectroscopy. *Chemical Engineering Research and Design*, 170, 213–223.
 558 <https://doi.org/10.1016/j.cherd.2021.04.003>

559 Ochsenein, D. R., Vetter, T., Schorsch, S., Morari, M., & Mazzotti, M. (2015). Agglomeration
 560 of needle-like crystals in suspension: I. Measurements. *Crystal Growth and Design*, 15(4),
 561 1923–1933. <https://doi.org/10.1021/acs.cgd.5b00094>

562 Patel, A. R., & Dewettinck, K. (2016). Edible oil structuring: An overview and recent updates.
 563 *Food and Function*, 7(1), 20–29. <https://doi.org/10.1039/c5fo01006c>

564 Patel, D., Patel, B., & Thakkar, H. (2021). Lipid Based Nanocarriers: Promising Drug Delivery
 565 System for Topical Application. *European Journal of Lipid Science and Technology*, 123(5),

566 1–12. <https://doi.org/10.1002/ejlt.202000264>

567 Povey, M. J. W. (2017). Applications of ultrasonics in food science - novel control of fat
 568 crystallization and structuring. *Current Opinion in Colloid and Interface Science*, 28, 1–6.
 569 <https://doi.org/10.1016/j.cocis.2016.12.001>

570 Pu, Y., Chaudhry, S., Parikh, M., & Berry, J. (2015). Drug Development and Industrial Pharmacy
 571 Application of in-line viscometer for in-process monitoring of microcrystalline cellulose-
 572 carboxymethylcellulose hydrogel formation during batch manufacturing Application of in-
 573 line viscometer for in-process monitoring of microcrystalline cellulose-
 574 carboxymethylcellulose hydrogel formation during batch manufacturing. *Drug Dev Ind*
 575 *Pharm*, 41(1), 28–34. <https://doi.org/10.3109/03639045.2013.845837>

576 Rathore, A. S., Bhambure, R., & Ghare, V. (2010). Process analytical technology (PAT) for
 577 biopharmaceutical products. *Analytical and Bioanalytical Chemistry*, 398(1), 137–154.
 578 <https://doi.org/10.1007/s00216-010-3781-x>

579 Rios, R. V., Pessanha, M. D. F., Almeida, P. F. de, Viana, C. L., & Lannes, S. C. da S. (2014).
 580 Application of fats in some food products. *Food Science and Technology (Campinas)*, 34(1),
 581 3–15. <https://doi.org/10.1590/s0101-20612014000100001>

582 Salami, H., McDonald, M. A., Bommarius, A. S., Rousseau, R. W., & Grover, M. A. (2021). In
 583 Situ Imaging Combined with Deep Learning for Crystallization Process Monitoring:
 584 Application to Cephalexin Production. *Organic Process Research and Development*, 25(7),
 585 1670–1679. <https://doi.org/10.1021/acs.oprd.1c00136>

586 Simone, E., Saleemi, A. N., & Nagy, Z. K. (2015). In situ monitoring of polymorphic

transformations using a composite sensor array of Raman, NIR, and ATR-UV/vis spectroscopy, FBRM, and PVM for an intelligent decision support system. *Organic Process Research and Development*, 19(1), 167–177. <https://doi.org/10.1021/op5000122>

Simone, Elena, Tyler, A. I. I., Kuah, D., Bao, X., Ries, M. E., & Baker, D. (2019). Optimal Design of Crystallization Processes for the Recovery of a Slow-Nucleating Sugar with a Complex Chemical Equilibrium in Aqueous Solution: The Case of Lactose. *Organic Process Research & Development*, 23(2), 220–233. <https://doi.org/10.1021/acs.oprd.8b00323>

Singh, A. P., McClements, D. J., & Marangoni, A. G. (2002). Comparison of ultrasonic and pulsed NMR techniques for determination of solid fat content. *JAOCS, Journal of the American Oil Chemists' Society*, 79(5), 431–437. <https://doi.org/10.1007/s11746-002-0501-y>

Singh, A. P., McClements, D. J., & Marangoni, A. G. (2004). Solid fat content determination by ultrasonic velocimetry. *Food Research International*, 37(6), 545–555. <https://doi.org/10.1016/j.foodres.2003.12.010>

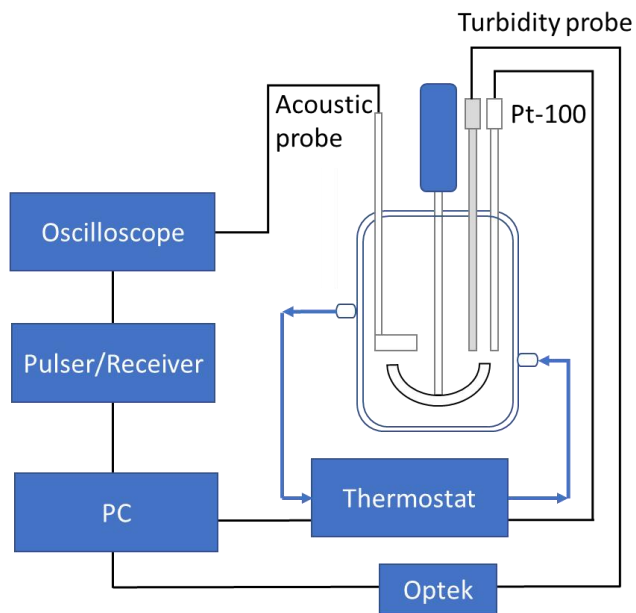
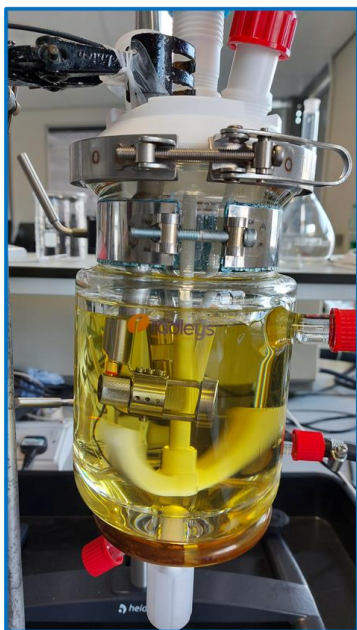
Szilágyi, B., & Nagy, Z. K. (2018). Aspect Ratio Distribution and Chord Length Distribution Driven Modeling of Crystallization of Two-Dimensional Crystals for Real-Time Model-Based Applications. *Crystal Growth & Design*, 18(9), 5311–5321. <https://doi.org/10.1021/acs.cgd.8b00758>

Tang, D., & Marangoni, A. G. (2008). Fractal dimensions of simulated and real fat crystal networks in 3D space. *JAOCS, Journal of the American Oil Chemists' Society*, 85(6), 495–499. <https://doi.org/10.1007/s11746-008-1237-7>

Titiz-Sargut, S., & Ulrich, J. (2003). Application of a protected ultrasound sensor for the

determination of the width of the metastable zone. *Chemical Engineering and Processing: Process Intensification*, 42(11), 841–846. [https://doi.org/10.1016/S0255-2701\(02\)00215-5](https://doi.org/10.1016/S0255-2701(02)00215-5)

Wasalathanthri, D. P., Rehmann, M. S., Song, Y., Gu, Y., Mi, L., Shao, C., ... Li, Z. J. (2020). Technology outlook for real-time quality attribute and process parameter monitoring in biopharmaceutical development—A review. *Biotechnology and Bioengineering*, 117(10), 3182–3198. <https://doi.org/10.1002/bit.27461>



616

617 Figure 1. Crystallization vessel fitted with a Pt-100 thermocouple, the turbidity probe and the
 618 custom ultrasound probe (left), schematic depiction of the rig used in this paper (right).

619

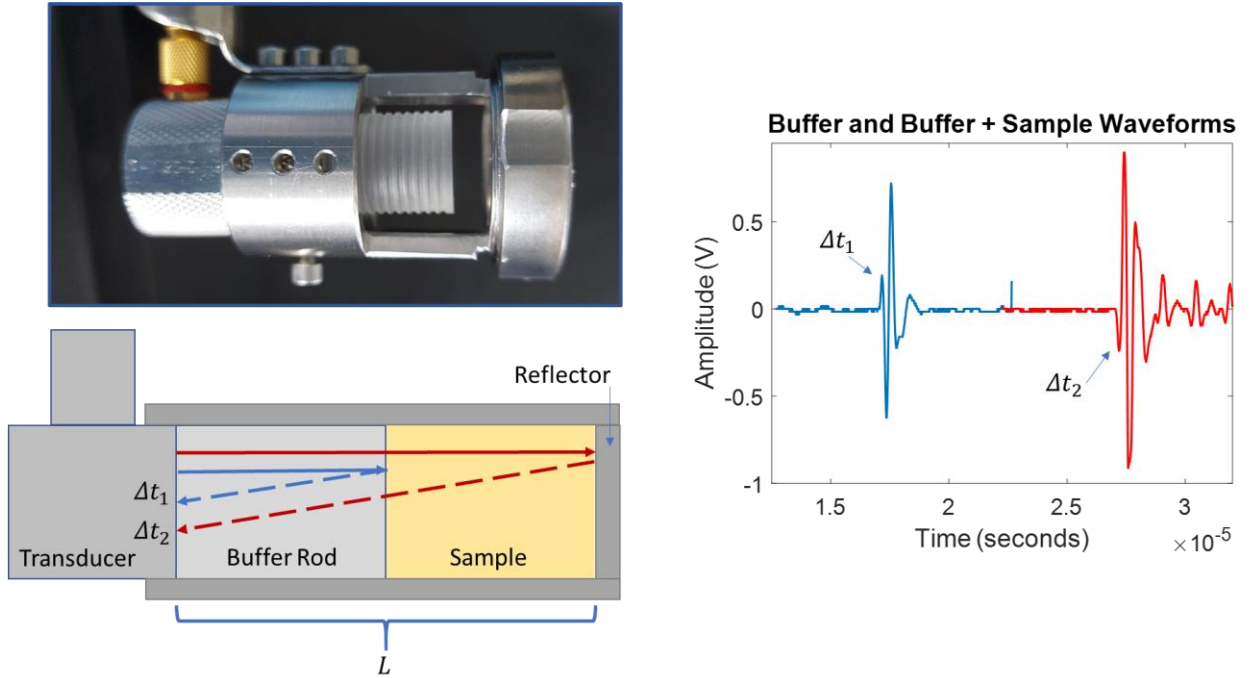


Figure 2. Schematic drawing of the custom acoustic probe (left) and the measured waveforms obtained by the reflection of the buffer rod (blue), and buffer rod and sample (red) (right). Δt_1 and Δt_2 represent the time-of-flight of the pulse travelling through the buffer rod and through the buffer rod and sample, respectively.

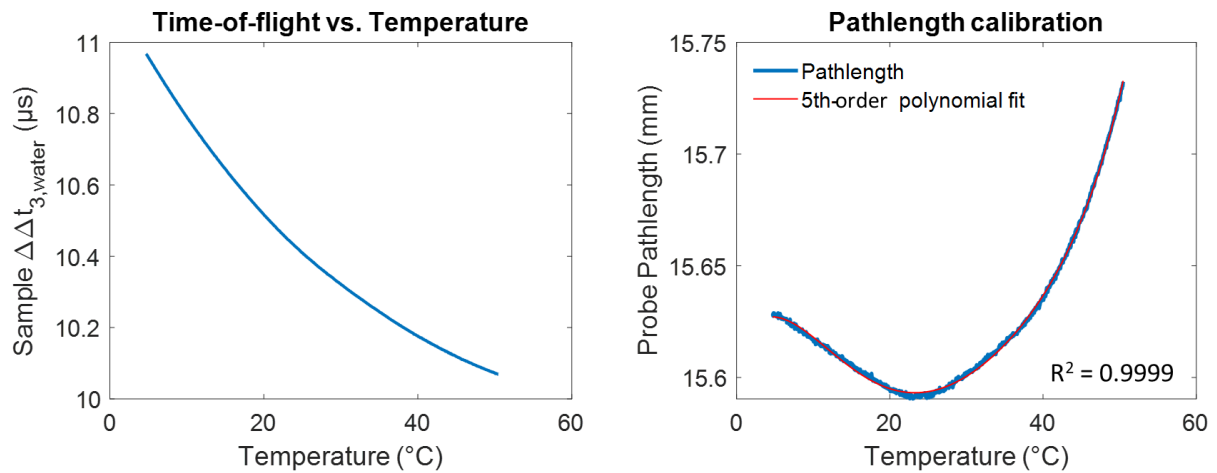


Figure 3. Measured time-of-flight in distilled water between 60 °C and 5 °C (left), calculated sample path length and 5th-order polynomial fitting (right).

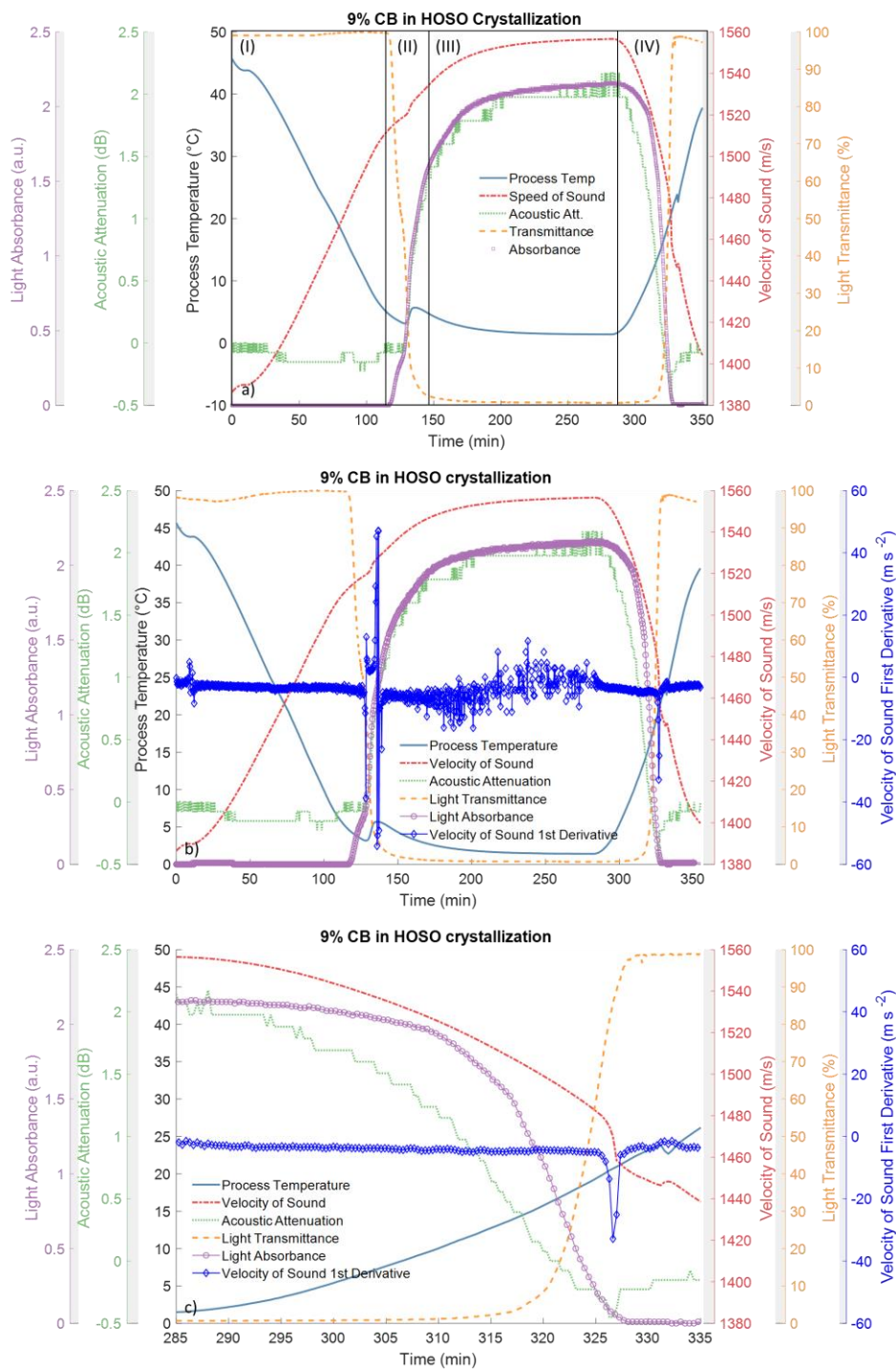


Figure 4. Process Analytical Technologies (PAT) tools plot of the crystallization of a 9% w/w CB in HOSO blend (a). The different regions of the crystallization process are indicated with roman numerals (I-IV). First derivative plot overlaid on the other PAT tools parameters (b) and

634 enlargement of the melting zone (c). Process temperature (-), velocity of sound (-·-), acoustic
635 attenuation (··), light transmittance (--), light absorbance (-o-) and first derivative of the velocity
636 of sound (-◇-) .

637

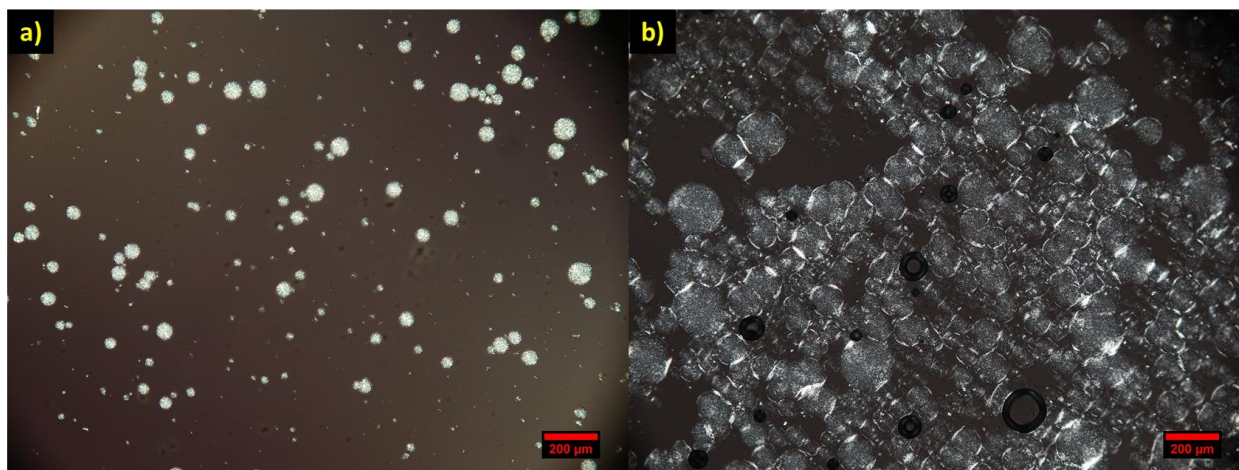
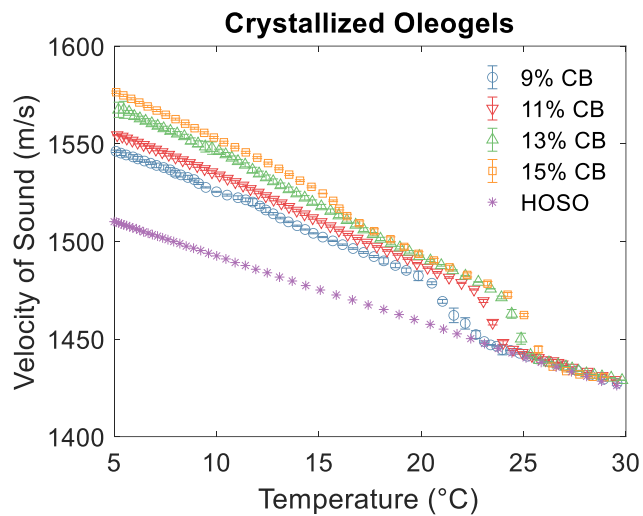
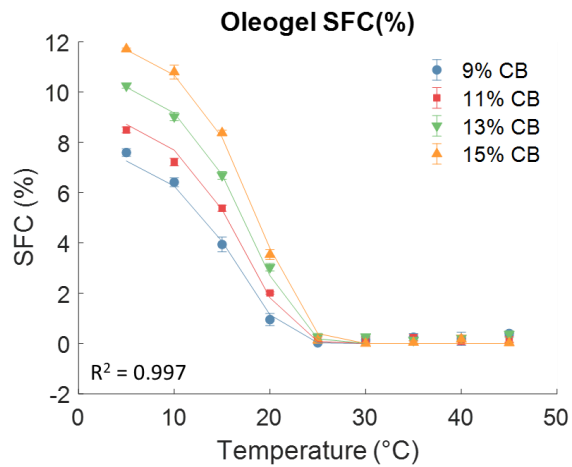


Figure 5. Polarized Light Microscopy (PLM) image of a 15% CB in HOSO mixture while crystallizing under shear. Onset of nucleation (a) and formation of the spherical aggregates network (b). Scale bar is 200 μm for both figures.



643
 644 Figure 6. Velocity of sound of crystallized CB/HOSO oleogels between 5 and 35 °C. The error
 645 bars show the standard deviation of three measurements for each concentration. The velocity of
 646 sound of the pure HOSO phase is also plotted for reference.

647



648

649 Figure 7. SFC% calculated with *p*NMR with respect to temperature for the different CB/HOSO
 650 blends. The datapoints were fitted using a Gompertz-type model, similar to the one described in
 651 Farmani (2015).

652

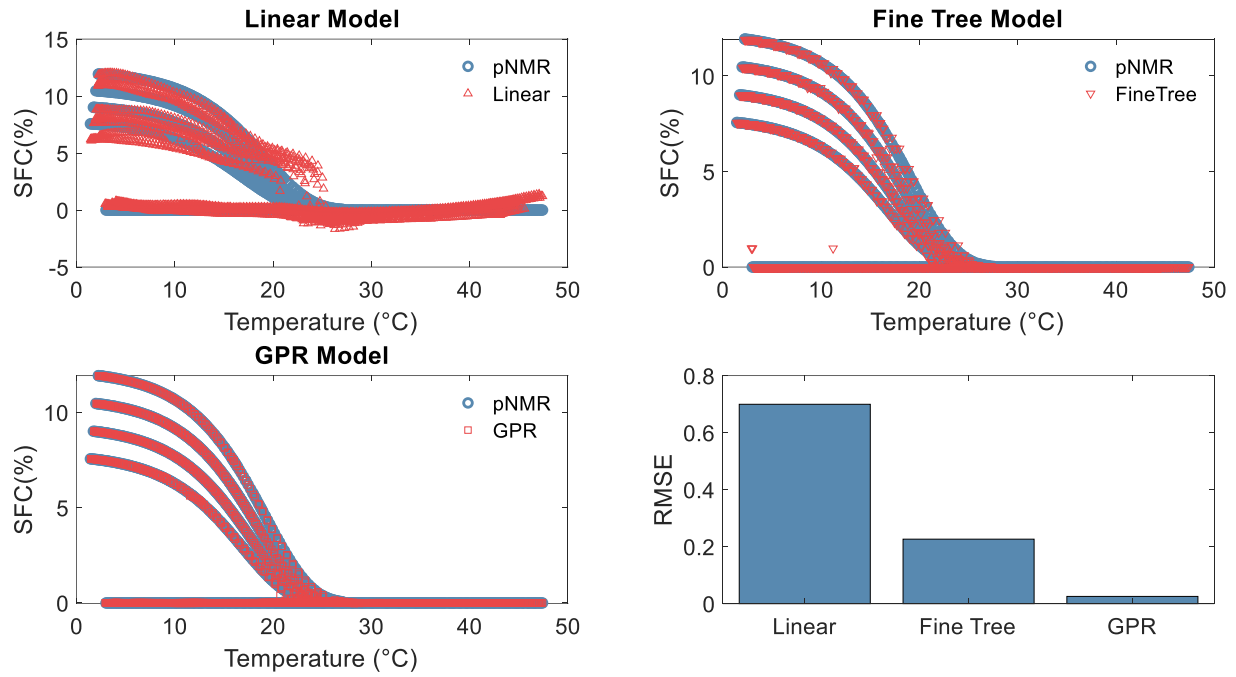
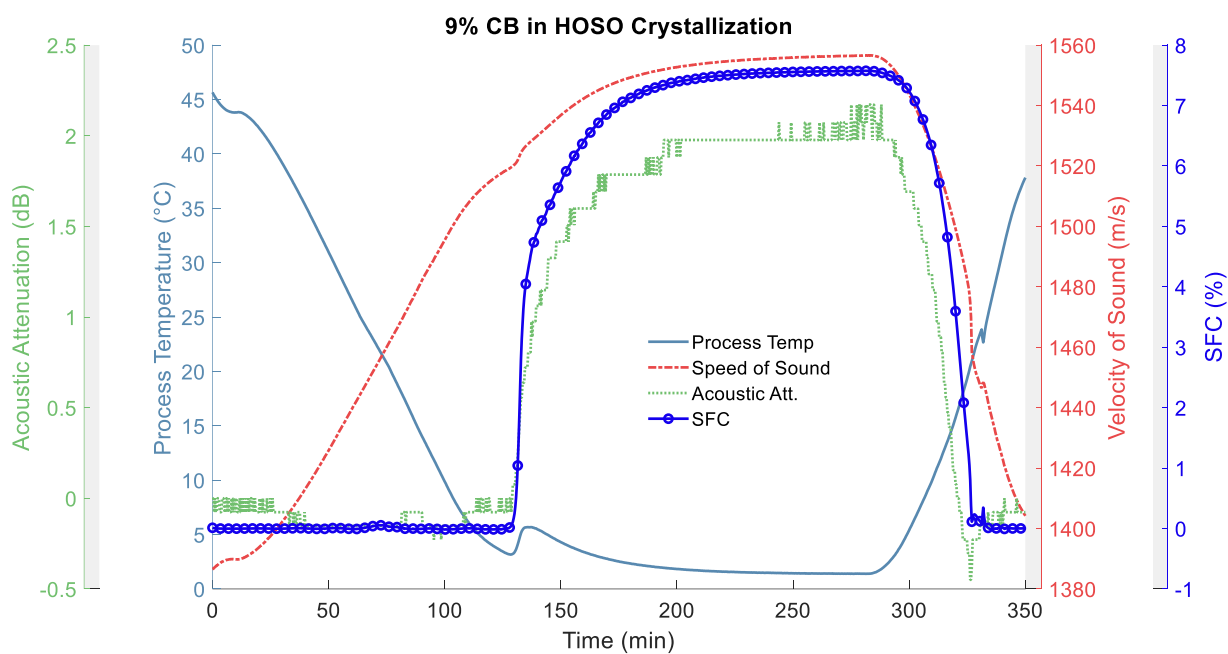


Figure 8. Predicted $SFC(\%)$ values obtained from the supervised-machine learning models, compared against the measured $SFC(\%)$ from $pNMR$ (blue circles) as a function of temperature: a) Linear model (red upward triangles), b) Fine Tree model (red downward triangles), c) Gaussian Process Regression (red squares) and d) histogram plot showing the RMSE on the $SFC(\%)$ values for each model.

660



661

662 Figure 9. Process Analytical Technologies (PAT) tools plot of the crystallization of a 9% w/w CB
 663 in HOSO blend. Process temperature (-), velocity of sound (-·-), acoustic attenuation (···), and
 664 predicted SFC% with the GPR model (-o-).

665

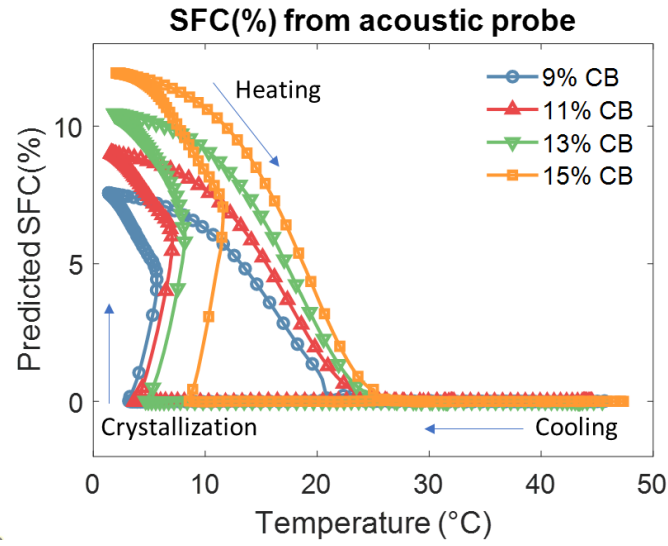


Figure 10. Evolution of ultrasound predicted SFC% during cooling from 40 °C to 5 °C and heating (5 °C to 40 °C) for oleogels containing different CB w/w %.

670

671 Table 1. Velocity of sound and acoustic attenuation for oleogel samples at the end of the
672 crystallization (5 °C).

CB % (w/w)	Velocity of Sound (5 °C) (m/s)	Acoustic Attenuation (5 °C) (dB)
9	1545.8 ± 2.2	2.25 ± 1.13
11	1555.1 ± 1.2	2.42 ± 0.09
13	1567.5 ± 6.5	2.61 ± 0.06
15	1578.6 ± 4.0	3.31 ± 0.42

673

674